AIP Advances

Simulation of diffusiophoresis force and the confinement effect of Janus particles with the continuum method

Meiling Wu, Hongyan Zhang, Xu Zheng, and Haihang Cui

Citation: AIP Advances **4**, 031326 (2014); doi: 10.1063/1.4868375
View online: http://dx.doi.org/10.1063/1.4868375
View Table of Contents: http://scitation.aip.org/content/aip/journal/adva/4/3?ver=pdfcov
Published by the AIP Publishing

AIP ADVANCES **4**, 031326 (2014)

Simulation of diffusiophoresis force and the confinement effect of Janus particles with the continuum method

Meiling Wu,[1] Hongyan Zhang,[1] Xu Zheng,[2] and Haihang Cui[1,a]
[1]*Xi'an University of Architecture and Technology, Xi'an, 710055, People's Republic of China*
[2]*Institute of Mechanics, CAS, Beijing, 100190, People's Republic of China*

(Received 14 November 2013; accepted 1 March 2014; published online 11 March 2014)

The Janus particle is a special class of colloidal particle that has different surface characteristics on its two hemispheres. In the microsystem field, an interesting application is the Janus particle's self-propulsion. Diffusiophoresis (DFP) provides one possible mechanism to explain this phenomenon. In this paper, we used the continuum model to simulate DFP and to study the confinement effect of Janus particles travelling on the substrate. In the experiment, we noticed a special quasi-1D motion, in which the DFP force is dominant and particles move at a constant velocity within a short interval approximately along a straight line. This enables us to adopt a reference frame to numerically study the distributions of the flow field and concentration field and hence to evaluate the different forces. Because the confinement effect has a great influence on the magnitude of forces, the gaps were calculated accurately according to the force balance principle. Meanwhile, the fitting coefficients to match the experimental and numerical results were suggested. This result may help us to get a better understanding of self-propulsion and is also beneficial for designing a DFP-based micro-device.
[http://dx.doi.org/10.1063/1.4868375]

I. INTRODUCTION

The Janus particle describes a special class of colloidal microspheres with different surface characteristics on its two hemispheres.[1] Among its applications, an interesting example is the movement of self-propulsion, wherein one hemisphere of the Janus particle is covered with a thin layer of metal catalyst (e.g. platinum, Pt) and serves to decompose the fuel reactants (e.g. $2H_2O_2 \rightarrow 2H_2O + O_2$). In MEMS and sensor fields,[2] because it has such a compact structure without an additional power supply, the self-propulsion of the Janus particle has attracted widespread attention. The phoretic motion due to this concentration gradient is called diffusiophoresis (DFP) (Fig. 1(a)).[3]

For the DFP model, Brady[4] and de Buyl[5] have put forward two theoretical descriptions from the continuum perspective and the colloid level. In the former, both solute and solution were treated as ideal uniform materials which were distributed continuously, and the "field" was used to depict the distribution. For the latter, the solute was treated as having the same role as Janus particles dispersed in a solvent. Although the different descriptions provide different mechanical analyses of phoretic motion, these two approaches agree very well when the solute is much smaller in size. With the continuum description, the DFP velocity of the Janus particle suspended in free space is given by the well-known theoretical expression:[4]

$$V_{th} = -\frac{1}{2}\frac{b^2}{\mu}k_B T \nabla n \tag{1}$$

[a]Corresponding author: Email: cuihaihang@xauat.edu.cn

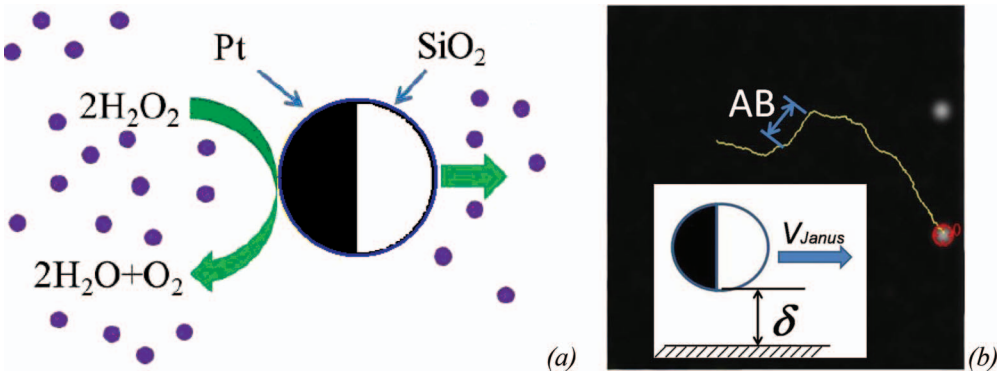

FIG. 1. Schematic of self-propulsion of Pt-SiO_2 particle driven by decomposing H_2O_2 (a) and the corresponding quasi-2D motion trajectory for Janus particle with $d = 2\ \mu$m (b).

where b is the hydrodynamic radius of the solute, μ is the dynamic viscosity of the solvent, k_BT is the thermal energy, and n is the number density of the solute. According to this equation, the phoretic particle will move along the direction from the high concentration region to the low concentration region.

At microscale, it was believed that self-propulsion was due to the competition between random Brownian motion and DFP motion.[6] Because the Brownian motion of a microparticle is inevitable, the motion information extracted from experimental observation includes not only the contribution from DFP motion but also that from Brownian motion, which means that the validity of DFP model cannot be accurately checked directly. In addition, the present DFP model seldom pays attention to the confinement effect of the near wall (Fig. 1(b)), which will also have a great influence on the DFP force.

In this paper, we started from the experimental measurement of Pt-SiO_2 Janus microspheres with a diameter of 2 μm. Three different stages, Brownian motion, DFP motion, and Brownian-like motion, were distinguished. Owing to the existence of the wall, particles were confined to moving in quasi-2D style. Especially, we found that for the second one, the DFP force became dominant and within a short interval the particle travelled at a constant velocity approximately along a straight line. Herein, the self-propellant motion became a quasi-1D motion, which provided us with the possibility of checking the DFP model and avoiding the effect of random motion. Therefore, we conducted the numerical solution with a continuum description, where a low Reynolds (Re) number flow, diluted species transport, and surface catalytic reaction were simulated. The effect of three kinds of fuel concentrations was considered for 2.5, 5, and 10% H_2O_2 solutions. Based on the force balance in the vertical and traveling directions, we obtained the distance δ between the particle and the substrate (Fig. 1(b)) and the confinement effect.

II. SELF-PROPULSION EXPERIMENT

A. Experimental measurement

The motion of a Pt-SiO_2 Janus microsphere with a diameter $d = 2.08 \pm 0.05\ \mu$m was observed thoroughly. E-beam evaporation was used to deposit a layer of Pt (thickness of about 7 nm) on the surface of one hemisphere of SiO_2 particles. Then, Janus particles were mixed into distilled water and a droplet of about 70 μl with different concentrations of H_2O_2 (2.5, 5, 10%) was dispensed onto a piece of glass slide. The particle trajectories were recorded by video microscopy. The whole experimental procedure is similar to that reported in Ke *et al.*[7] and Ebbens and Howse.[8] However, some special measures were taken to improve the accuracy and repeatability of our experiment, for example the use of a fresh sample solution, steady ambient environment, and special imaging processing for the Janus particles. The motion of the particles was analyzed using the particle-tracing method. With the image series obtained, we can extract the position information of self-propellant

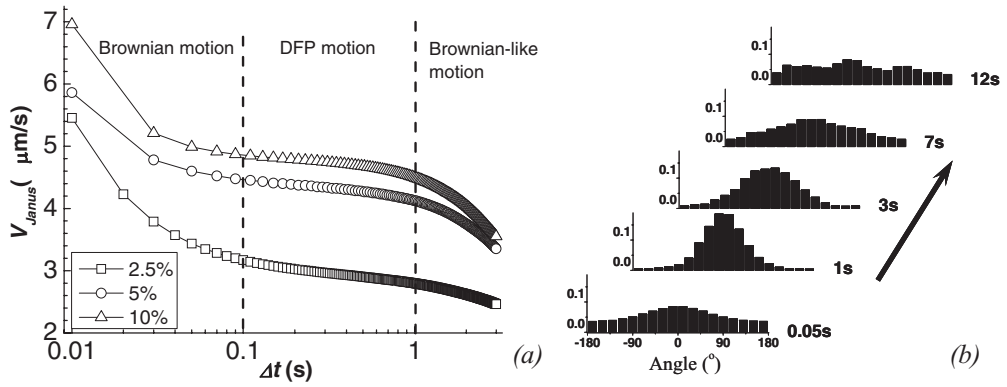

FIG. 2. Particle velocity V_{Janus} for three different H_2O_2 solutions (a) and displacement rotation angle for 2.5% H_2O_2 solution (b) as a function of the observation time interval Δt for a Janus particle with $d = 2$ μm.

Janus particles at different times and further calculate their trajectory, mean-square displacements, velocity, and effective diffusion coefficients. More than 10^3 particles and up to 10^5 images were taken for each operation condition. More details can be found in our previous work.[9]

B. Motion analysis of self-propulsion

The typical trajectory of a Janus particle is shown in the inset of Fig. 1(b). From the top view, it can be seen that at short times the particle appears to show directed motion, such as segment *AB* shown in Fig. 1(b); at longer times, the direction of motion becomes randomized. Two quantitative methods are used to depict this motion, as shown in Fig. 2. The first one is the curve of the average velocity of the Janus particle V_{Janus} versus the observation time Δt (Fig. 2(a)). It can be seen that in the left sub-region ($\Delta t < 0.1$ s) and right sub-region ($\Delta t > 1$ s), V_{Janus} decreases with the increase of Δt; only in the middle sub-region (0.1 s $< \Delta t <$ 1 s) is V_{Janus} almost a constant (3, 4.4, and 4.8 μm/s for 2.5, 5, and 10% H_2O_2 solution respectively). The second method uses the probability of the displacement rotation angle (Fig. 2(b)). It can be seen that the motion at $\Delta t = 0.05$ s is random because the probability of each angle is approximately equal; the motions after $\Delta t = 1$ s become directional because the probabilities of the angles are uneven and a notable peak appears near zero; when Δt approaches 12 s, the motion recovers to the random state because the probabilities of each angle become equal again and the peak disappears. For clarity, only the data for the 2.5% H_2O_2 solution are given. From Fig. 2, it is concluded that for the self-propulsion in our experiment there are three different stages: Brownian motion, DFP motion, and Brownian-like motion.

The reason why three motions happen can be explained simply from the orders of different forces. For a bare SiO_2 particle undergoing a classic Brownian motion, the Brownian force $F_{Brownian}$ describing the strength of stochastic force applied by the surrounding small solvent molecules is:[10]

$$F_{Brownian} = \xi \sqrt{\frac{12\pi k_B T \mu R_p}{\Delta t}} \tag{2}$$

where ξ is a random number, R_p is the radius of the particle, and Δt is the time interval. This expression clearly shows that the strength of the Brownian force $F_{Brownian}$ decreases with the increase of Δt. Thus, for an unchanged F_{DFP}, the relative importance of $F_{Brownian}$ becomes weakened as the observation time Δt increases. However, in consideration of the accumulation effect of the rotation angle ($\Delta\theta \sim \sqrt{\frac{3k_BT}{16\pi\mu R_p^3}} \cdot \Delta t^{1/2}$), randomness of the particle motion will appear again when the observation time Δt is large enough (about 10 s or higher). This kind of random motion has a stronger diffusive ability and is named Brownian-like motion. In this paper, we only paid attention to F_{DFP}-dominated motion.

From the experimental observation, it was also believed that the motion of a Janus particle is a quasi-2D translational motion. From the videos recorded under microscopy, the interface of the

Pt-side and SiO_2-side can be distinguished clearly and the direction of the interface was vertical to the substrate plane (Fig. 1(b)). During the entire process, the Janus particle always kept the same position and no rotation was observed, which proves that the Janus particle is experiencing a translational motion. Secondly, because the particle trajectory is clear all of the time, it is suggested that the vertical positions of particles are always within the focal plane of microscopy and Janus particles do not jump away from the substrate.

In summary, a Janus particle moving on the substrate experiences a quasi-2D motion in the XY plane. Typically, for an F_{DFP}-dominated motion, it becomes a quasi-1D motion. As is well known, for a translational motion, the gap δ between particle and substrate has a great influence on the hydrodynamic force.[11] And this strong dependence on the gap is also suitable for a DFP force. Unfortunately, when a particle is moving on the substrate, it is difficult to decide the gap accurately experimentally. In the following part, we will focus on this F_{DFP}-dominated quasi-1D motion and try to clarify the confinement effect for DFP.

III. CONTINUUM SIMULATIONS OF DIFFUSIOPHORESIS

A. Governing equation and boundary conditions

Generally, the quasi-2D motion of a spherical particle is time-dependent in a global frame. But, the governing equations can be solved in a reference frame fixed on the particle and in this frame the computation around the particle becomes time-independent. The governing equations for a steady-state, force-free particle with low *Re* is:

$$\begin{cases} \nabla U = 0 \\ \mu \nabla^2 U = \nabla \mathrm{p} \end{cases} \tag{3}$$

The hydrodynamic force F_{Stokes} is expressed as the surface integration on the particle:

$$F_{Stokes} = \iint_A \Pi e_r dS \tag{4}$$

where e_r is the radial unit vector and dS is the surface area element on the spherical surface. $\Pi = -p + \mu \sum$ is the pressure tensor, p is the hydrostatic pressure, and $\sum$ is the shear stress tensor.

Similarly, the governing equations for steady-state diluted species transport are:

$$\partial_t n + U \nabla n - D \nabla^2 n = 0 \tag{5}$$

Here D is the diffusive coefficient. Different D for H_2O_2, H_2O, and O_2 are 1.4×10^{-9}, 2.37×10^{-9}, and 2.3×10^{-10} m^2 s^{-1}, respectively. In principle, F_{DFP} can be expressed as a similar surface integration on the particle to F_{Stokes}. Combining Eq. (1) and the Stokes assumption at low *Re* number, the corresponding F_{DFP} is expressed as:

$$F_{DFP} = 6\pi c_{DFP} R_p \mu V_{th} = -3\pi c_{DFP} R_p b^2 k_B T \frac{N_A \iint_A \nabla C e_r dS}{A} \tag{6}$$

Here A is the surface area of the particle, N_A is Avogadro's constant, and c_{DFP} is the correction factor that matches the possible difference between the theoretical value of Eq. (1) and the present experimental measurement. Note that in the above equation, n, the number density of solute in Eq. (1), is replaced by C, the local molar concentration obtained from the numerical result. For the present case, $R_p = 1 \times 10^{-6}$ m, $b = 0.62 \times 10^{-10}$ m, $\mu = 1.002 \times 10^{-3}$ Pa.s, $k_B = 1.38 \times 10^{-23}$ J/k, and $T = 293$ k.

The numerical simulation was conducted on a Comsol Multiphysics 4.1 platform. The Janus microsphere is placed at the bottom of a cubic box with a size of $50 \times 50 \times 40$ μm. The vertical position of the particle is adjustable. In the reference frame, the quiescent fluid flow becomes $-V_{Janus}$. The corresponding boundary conditions on the left-hand and right-hand sides of the computational

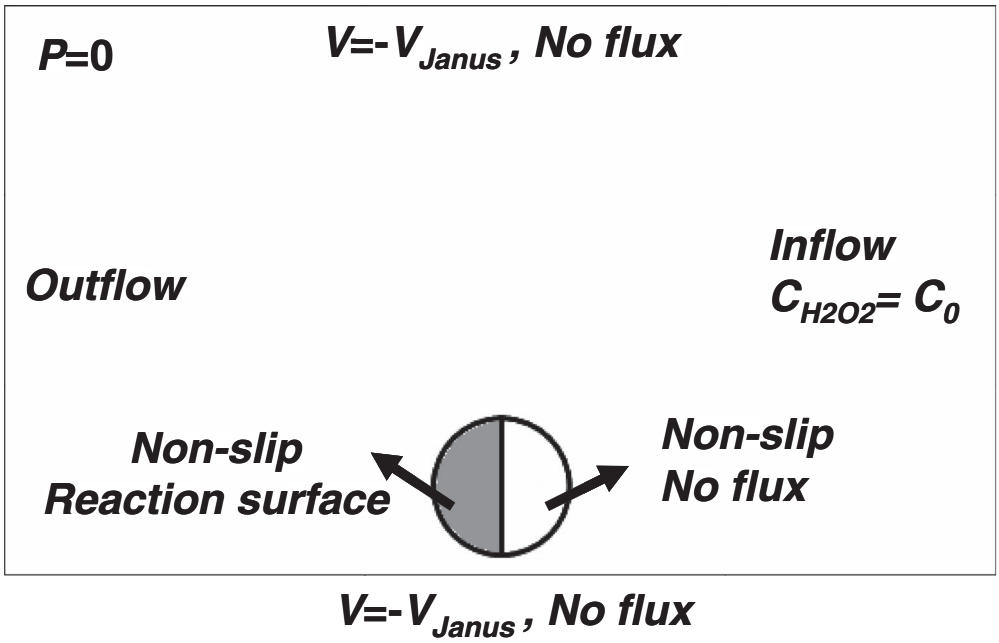

FIG. 3. Boundary conditions for the numerical simulation (not to scale).

domain are inflow or outflow with zero stress. On the surface of the Janus particle, a non-slip boundary is applied (Fig. 3).

For the diluted species transportation model, the right-hand side shows the inflow, with a concentration C_0 of 737.4 mol/m^3 (for 2.5% H_2O_2), 1488.5 mol/m^3 (for 5% H_2O_2), or 3033.2 mol/m^3 (for 10% H_2O_2), and the left-hand side shows the outflow. The Pt-side of the Janus particle is a reaction surface with the inward flux decided by H_2O_2 catalysed decomposition. Other boundaries, including the SiO_2 side of the Janus particle, top/bottom surfaces, and front/back surfaces, have no flux. As reported in the literature,[8,12] the Pt-catalysed breakup of H_2O_2 occurs in two stages. Firstly, H_2O_2 molecules are absorbed on the surface of the catalyst at a rate k_1 and then H_2O_2 molecules are decomposed into water and oxygen at a rate k_2. For the whole, the integrated reaction rate k is

$$k = k_2 \frac{[H_2O_2]_{vol}}{[H_2O_2]_{vol} + k_2/k_1} \tag{7}$$

Here $[H_2O_2]_{vol}$ is expressed in units of volume percentage, k_1 is 48.1728 mol/m^{2}s, and k_2 is 5.1495 mol/m^{2}s. The resultant k is about 0.9767 mol/m^{2}s (for 2.5% H_2O_2), 1.6412 mol/m^{2}s (for 5% H_2O_2), and 2.4884 mol/m^{2}s (for 10% H_2O_2).[13]

On the Comsol Multiphysics platform, an ideal reactor model for a H_2O_2 catalytic reaction was constructed first, which assumes by default that reactions take place in the entire reactor volume. Then, a space-dependent model was created by the system automatically when the real 3D microreactor model, where the reaction occurs at the catalytic surfaces, was created. The boundary fluxes at the catalytic surfaces are decided by the outer concentration, which is transferred to the ideal reactor model from the 3D microreactor model in real-time, and the integrated reaction rate k, which has been assigned in the ideal reactor model at the initial stage. Please refer to the Comsol Multiphysics 4.3a Manual for more details.[14]

B. Balance of forces

As stated above, we have chosen the F_{DFP}-dominated quasi-1D motion. Therefore, only the balances of forces in the X-direction (translational direction) and Z-direction (gravity direction) are considered. Related forces include the hydrodynamic force F_{Stokes}, the effective gravity G_{eff} (the

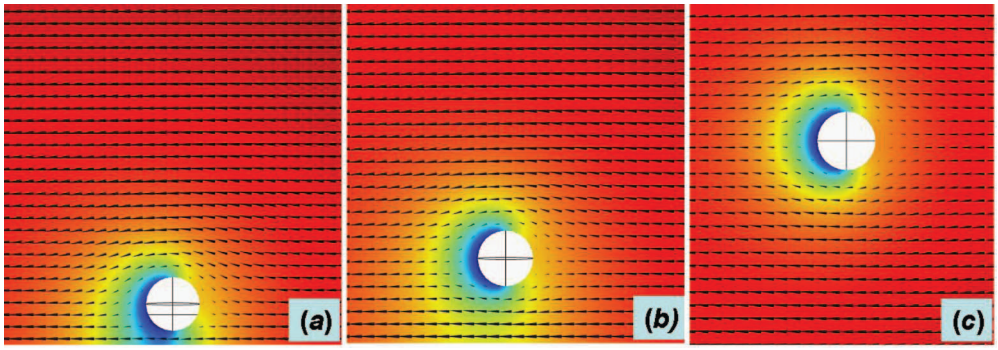

FIG. 4. Distributions of flow velocity (arrow) and H_2O_2 concentration (color) around a Janus particle located above the substrate in three different positions: $\delta = 0.5$ μm (a), $\delta = 2$ μm (b), and $\delta = 20$ μm (c) for 2.5% H_2O_2.

sum of buoyancy and gravity, 6.8×10^{-14} N for this case), and F_{DFP}. Other forces are negligible. For Janus particles of microsize, rticles would reach their terminal velocity immediately. Thus, two equations are constructed as below:

$$\begin{cases} X : F_{Stokes-X}(\delta, v) + F_{DFP-X}(\delta, v) = 0 \\ Z : F_{Stokes-Z}(\delta, v) + F_{DFP-Z}(\delta, v) - G_{eff} = 0 \end{cases} \tag{8}$$

Here, the sign of G_{eff} is negative because the effective gravity points to the negative Z-direction. In this problem, both the velocity distribution and the concentration distribution are strongly dependent on the unknown gap δ.[11] Besides the variable δ, there is another variable c_{DFP} that is undecided. In total, the numbers of equations and variables are the same and this is a well-posed problem. We need to test different gaps and c_{DFP} to find the proper values that satisfy the above two equations at the same time.

C. Velocity and concentration distributions

In Fig. 4(a), the distribution of flow velocity is given for the particle with a 0.5 μm gap. From this figure, it can be seen that the velocity far from the particle equals V_{Janus} and the velocity on the particle surface is zero. In the flow direction, the magnitude of velocity is symmetrical about the axis vertical to the flow direction. This symmetrical distribution is due to the nature of low *Re* flow. In the vertical direction, the unsymmetrical boundary condition results in an unsymmetrical distribution of the velocity field. The average velocity is higher at the top than at the bottom. Therefore, there is a very large shear rate across the particle, which may induce a significant lift force.

The distribution of H_2O_2 concentration in this confinement space is also shown in Fig. 4(a). The influent concentration of H_2O_2 solvent is 2.5%, which means that the concentration far from the particle equals the initial concentration of $C_0 = 737.35$ mol/m^3. Because the Janus particle is placed along the flow direction and the Pt-side is located downstream, the concentration at the upstream side does not change, obviously. The decomposition of H_2O_2 happens at the downstream side, where the H_2O_2 molecule touches the Pt layer. The lowest concentration (about 14.24 mol/m^3) is found on the Pt surface. Due to the existence of the wall, the concentration field also becomes unsymmetrical. The average concentration at the top is higher than that at the bottom, which is reasonable because the lower velocity at the bottom will provide more time to trigger the reaction of H_2O_2. For simplicity, we did not draw the distribution of product molecules of H_2O and O_2 in Fig. 4; nevertheless, it is straightforward to deduce from the distribution of H_2O_2. The more H_2O_2 molecules are reacted, the more molecules of O_2 and H_2O are generated. The opposite trends should also be observed.

In order to study the effect of confinement, we also tried different particle positions. In Figs. 4(a) to 4(c), the vertical positions of the Janus particles are raised gradually. It can be seen that with the increase of δ, the concentration distribution of H_2O_2 becomes more symmetrical about the flow direction. We calculated the integration of the H_2O_2 concentration gradient over a spherical

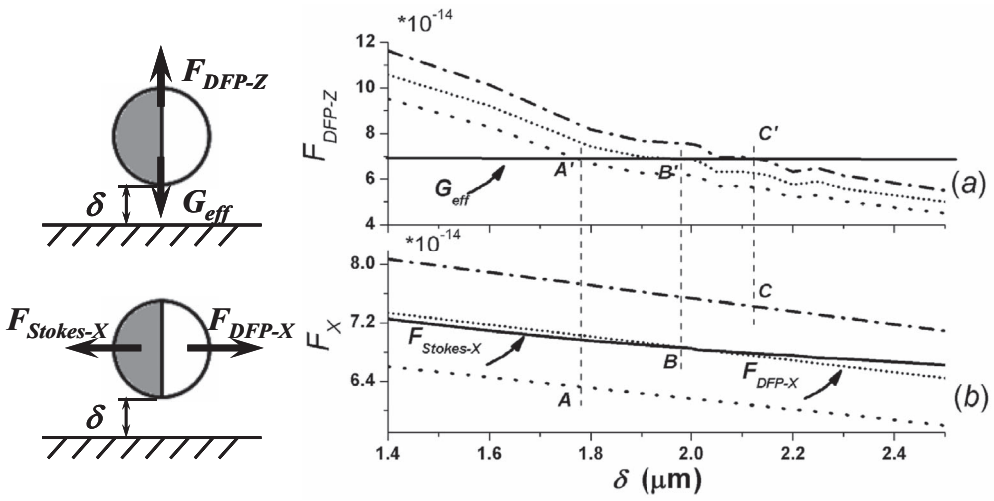

FIG. 5. Schematic of force balance in the *X*- and *Z*-directions and the calculation of the particle position δ and the diffusiophoretic force F_{DFP} for 2.5% H_2O_2.

surface for three different cases. The integrations of ∇C_X (the differential of C in the X-direction) are 2.19×10^{-4}, 1.30×10^{-4}, and 1.28×10^{-4} mol.m^{-2}, respectively. The first case ($\delta = 0.5\ \mu$m) is about 1.7 times higher than the last case ($\delta = 20\ \mu$m). The integrations of ∇C_Z (the differential of C in Z-direction) are 5.53×10^{-4}, 1.65×10^{-4}, and 7.83×10^{-6} mol.m^{-2}. Unlike the situation in the X-direction, the gradient value of the Z-direction for the confinement space (Fig. 4(a)) is several orders higher than that of the free space (Fig. 4(c)). All signs of the above results are positive, which means that F_{DFP} will point to the positive X- or Z-direction under the present condition. It is also noted that the above values have the same order ($\sim 10^{-4}$) in different directions. Therefore, it is suggested that two components of F_{DFP} in the X- and Z-directions will have equal importance for the movement of the Janus particles.

D. Diffusiophoretic force

Once the distributions of velocity and concentration have been obtained, F_{Stokes} and F_{DFP} can be evaluated using Eqs. (4) and (6), respectively. Prior to solving, the effect of the Z-component of F_{Stokes} has to be considered. Through the integration for the Stokes drag, the result shows that the component of F_{Stokes} in the Z-direction ($\sim 10^{-18}$ N) is about four orders of magnitude smaller than that of the effective gravity G_{eff} ($\sim 10^{-14}$N), which means that the Z-component of F_{Stokes} does not play a key role in the force balance of this direction. The force balance is from G_{eff} and $F_{DFP\text{-}Z}$. Next, by adjusting the gap δ and the match coefficient c_{DFP}, we may obtain the different values of F_{Stokes} and F_{DFP}. The illustrative curves of $F_{Stokes\text{-}X}$, $F_{DFP\text{-}X}$, and $F_{DFP\text{-}Z}$ as a function of δ and c_{DFP} are plotted in Fig. 5.

To decide which values of δ and c_{DFP} are suitable for the present experiment, we introduced the intersection method. We assume that there are three different c_{DFP} and at least one of them is corrected. The curves for $F_{DFP\text{-}X}$, $F_{DFP\text{-}Z}$, and $F_{Stokes\text{-}X}$ as a function of δ are drawn as shown in Fig. 5 first. For the known G_{eff} (solid line), there are three intersection points (A', B', and C') with the curve of $F_{DFP\text{-}Z}$. Each intersection point represents the fact that at that position the force balance condition in the Z-direction has been satisfied. From these intersection points, it is straightforward to decide three different values of δ accordingly. But, the correct δ has to satisfy the force balance in the X-direction at the same time. Next, the points A, B, and C related to A', B', and C' are decided by drawing a perpendicular line to intersect with the $F_{DFP\text{-}X}$ curve in Fig. 5(b). However, it is found that only point B is exactly at the intersection of $F_{DFP\text{-}X}$ and $F_{Stokes\text{-}X}$, which means that the situation corresponding to point B also satisfies the force balances in the X-direction. Therefore, the correct values of δ and c_{DFP} are found.

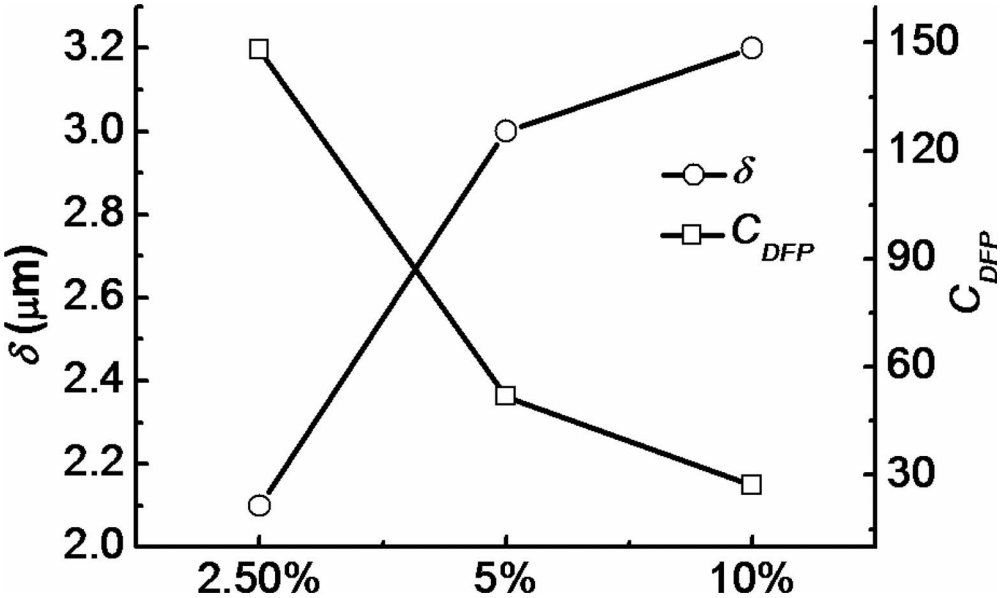

FIG. 6. Values for δ and c_{DFP} in H_2O_2 solution of different concentrations.

In this paper, for the different concentrations of H_2O_2 solution (2.5, 5, 10%), the values of δ are 2.1, 3.0, and 3.2 μm, respectively (Fig. 6). This result is in agreement with the experimental observation (1∼4 μm).[9] The fitting coefficient c_{DFP} can be decided from the curve that passes through point B' in Fig. 5(a). The values of coefficient c_{DFP} are 147.9, 51.8, and 27.2 for the 2.5, 5, and 10% H_2O_2 solutions, respectively (Fig. 6). Note that for simplicity, these coefficients are evaluated based on the gradient of H_2O_2 concentration directly rather than on the gradient of all solute molecules (H_2O_2, H_2O, O_2). With this processing mode, the sign in Eq. (6) should be positive instead of negative.

IV. DISCUSSION AND CONCLUSIONS

We have introduced a numerical method to study *DFP* and the confinement effect of a Janus particle that is travelling on the substrate. Through testing different values of δ, the confinement effect is confirmed. However, there are still some drawbacks for the numerical simulation. The Comsol Multiphysics platform is based on the finite element method, which is able to provide a stable and reliable solution but is not very suitable to treat a near-wall flow problem. More robust CFD methods such as the immersed boundary method or boundary element method are suggested for future works. Among all parameters, the reaction rate constant is a key parameter and ranges from about 10^{-3} to 10^{-8} m s^{-1} as the concentration of H_2O_2 increases from zero to 30%. Choosing the correct value is difficult because this process is controlled by many parameters. Therefore, it is believed that this inaccurate reaction rate constant could be the reason why the match coefficient obtained in this paper is not so reasonable. In the simulation, we also neglected the reaction heating and the change of property parameters (i.e. viscosity and diffusive coefficient) due to the change of composition, which may lead to inaccurate results and will be improved in future works.

In summary, we conducted experimental observations first and distinguished three different stages according to the velocities of Janus particles and the probabilities of displacement rotation angles. The middle one was deemed to be a suitable situation to provide the basic data, where the random Brownian motion was suppressed. Through the simulation, we obtained the distribution of the flow field and concentration field and hence obtained the forces by surface integration over the sphere's surface. We proposed the intersection method to decide on suitable parameters. The position that has the intersection in both the *X*- and *Z*-directions is the correct value, and also represents the balance of force in the *X*- and *Z*-directions at the same time. The obtained values for the gap are

about 2.1∼3.2 μm and the match coefficient is about 147.9∼27.2. Based on these parameters, it can be seen that the DFP force is quite different from the value predicted by the classical theory, which could result from the confinement effect and the oversimplified theoretical model. This will help us to get a better understanding of the DFP mechanism and to design DFP-based microdevices in the future.

ACKNOWLEDGMENTS

This work is funded by the National Natural Science Foundation of China (Grant Nos. 21005058, 11272322, and 11202219), the Specialized Research Fund for the Doctoral Programme of Higher Education of China (Grant Nos. 20106120120011), and the Shaanxi Provincial Department of Education Special Research Programme (Grant No. 11JK0530). The authors gratefully acknowledge Prof. Chen Li-Guo and Dr Xu Xiao-Wei from Soochow University for their kind help in using their microfabrication facilities.

[1] S. Granick, S. Jiang, and Q. Chen, "Janus particles," Physics Today **62**, 68 (2009).
[2] R. Kapral, "Perspective, nanomotors without moving parts that propel themselves in solution," Journal of Chemical Physics **138**, 020901 (2013).
[3] H. Brenner, "Phoresis in fluids," Physical Review E **84**, 066317 (2011).
[4] J. F. Brady, "Particle motion driven by solute gradients with application to autonomous motion: continuum and colloidal perspectives," Journal of Fluid Mechanics **667**, 216–259 (2011).
[5] P. de Buyl and R. Kapral, "Phoretic self-propulsion: a mesoscopic description of reaction dynamics that powers motion," Nanoscale **5**, 1337–1344 (2013).
[6] J. R. Howse, R. A. L. Jones, A. J. Ryan, T. Gough, R. Vafabakhsh, and R. Golestanian, "Self-motile colloidal particles: from directed propulsion to random walk," Physical Review Letters **99**, 048102 (2007).
[7] H. Ke, S. Ye, R. L. Carroll, and K. Showalter, "Motion analysis of self-propelled Pt-silica particles in hydrogen peroxide solutions," Journal of Physical Chemistry A **114**, 5462–5467 (2010).
[8] S. J. Ebbens and J. R. Howse, "Direct observation of the direction of motion for spherical catalytic swimmers," Langmuir **27**, 12293–12296 (2011).
[9] X. Zheng, B. ten Hagen, A. Kaiser, M. L. Wu, H. H. Cui, and Z. H. Sliber-Li, "Non-Gaussian statistics for the motion of self-propelled Janus particles: Experiment versus theory," Physical Review E **88**, 032304 (2013).
[10] M. Kim and A. L. Zydney, "Effect of electrostatic, hydrodynamic, and Brownian forces on particle trajectories and sieving in normal flow filtration," Journal of Colloid and Interface Science **269**, 425–431 (2004).
[11] H. Lee, M. Y. Ha, and S. Balachandar, "Rolling/sliding of a particle on a flat wall in a linear shear flow at finite Re," International Journal of Multiphase Flow **37**, 108–124 (2011).
[12] S. B. Hall, E. A. Khudaish, and A. L. Hart, "Electrochemical oxidation of hydrogen peroxide at platinum electrodes. Part 1. An adsorption-controlled mechanism," Electrochimica Acta **43**, 579–588 (1997).
[13] S. Ebbens, M. H. Tu, J. R. Howse, and R. Golestanian, "Size dependence of the propulsion velocity for catalytic Janus-sphere swimmers," Physical Review E **85**, 020401 (2012).
[14] Comsol Multiphysics 4.3a Manual. Chemical reaction engineering model. Hydrocarbon dehalogenation in a tortuous microreactor.